Electron scattering studies of BF and BF_2

Dhanoj Gupta[1,2], Heechol Choi[1], Mi-Young Song[1], Suvam Singh[3], Bobby Antony[3], Kalyan Chakrabarti[4], Jung-Sik Yoon[1] and Jonathan Tennyson[5]

[1]Plasma Technology Research Center, National Fusion Research Institute, 37 Dongjangsan-ro, Gunsan, Jeollabuk-do 54004, South Korea
[2] Department of Particle Physics and Astrophysics, Weizmann Institute of Science, Rehovot 7610010, Israel
[3] Atomic and Molecular Physics Lab, Department of Physics, Indian Institute of Technology (Indian School of Mines), Dhanbad, JH 826004, India
[4] Department of Mathematics, Scottish Church College, 1 & 3 Urquhart Sq, 700 006 Kolkata, India
[5] Department of Physics and Astronomy, University College London, Gower Street, London WC1E 6BT, UK

E-mail: dhanojsanjay@gmail.com

April 2020

Abstract. The present article reports calculated elastic, differential, momentum transfer and excitation cross section for electron scattering from BF and BF_2 radicals using the *ab-initio* R–matrix method. The calculations are performed with complete active space – configuration interaction and static exchange models for both targets to yield scattering cross sections and resonance parameters. Elastic and momentum transfer cross sections are also calculated using the spherical complex optical potential method to cover a wide energy range. The total ionization cross section is also reported from ionization threshold to 5 keV. The calculated cross sections for these neutral species are important for BF_3 plasma and are reported for the first time to the best of our knowledge except ionization.

1. INTRODUCTION

Electron scattering studies of the neutral radicals BF and BF_2 are important for BF_3 plasma. However, to the best of our knowledge there has been little experimental or theoretical investigation on electron scattering from these radicals. BF_3 plasmas generated from arc, pulsed or RF/ECR discharge are used as a boron source, which in turn is widely used as a p–type dopant in the ion implantation for the semiconductor industry [1–3]. The halogen-containing gaseous BF_3 is important for a variety of plasma technologies and finds applications in the field of material processing, plasma-assisted fabrication of large integrated circuits and semiconductor fabrication [4]. The interaction of free electrons in a BF_3 plasma generates different active neutral species such as B,

BF, BF_2, BF_3 and positive ion species such as B^+, BF^+, BF_2^+, BF_3^+. Such collision processes also govern the stability and discharge equilibrium of the plasma. The species generated and free electrons in the plasma give rise to various collisional processes whose understanding is important for modelling BF_3 plasma. Reliable electron collision cross sections for all species of ions and neutrals present in the plasma are therefore important data for performing plasma discharge simulations accurately.

The collision cross section data are essential input to plasma simulations, and the accuracy of such simulations are directly related to the reliability of input data. The collision cross section data in the range (3∼100 eV) are important for low-temperature plasmas ($3 \sim 5$ eV), where the energy of electron can be distributed up to 100 eV. Elastic scattering is the dominant process in most plasma discharges as the collision cross section for this process is large compared to other reactions; elastic scattering helps to thermalise the electrons. On the other hand for the electronic excitation processes, the threshold for electronic excitation is lower than the ionization threshold, so this reaction can be important when the electron temperature is low. In an experiment, the scattering and excitation cross sections can be used to analyze electron heating mechanism [5, 6]. Even in this case, data is required to a minimum of 25 eV, but up to a maximum of 100 eV are desirable. Moreover, the experimental studies of radicals such as BF and BF_2 are difficult and rare as these radicals are hard to prepare, highly reactive and powerful etchants; hence there are no experimental data available at present. The importance of theoretical calculations in providing data over a comprehensive range of energies is well established [7].

Considerable attention has been given to electron collision studies with neutral BF_3 molecule both theoretically and experimentally [4, 8–17]. There are also a few electron collision studies on positive BF_x ions for various collision processes in the literature [1, 18, 19]. However, there has been no systematic study of electron-induced collision processes in the radical species BF and BF_2, which play an important role in any BF_3 containing plasma. Our recent study [17] on electron scattering cross section of BF_3 molecule using the R–matrix method showed good agreement with the experimental data, which encouraged us to perform similar calculations on BF and BF_2. This is one of the major motivations for the present work. The only study available in the literature is due to the work of Kim and co-workers [10] who have provided ionization cross sections for BF and BF_2 using the Binary Encounter Bethe (BEB) [20] method. Hence, In the present work, we have provided a set of important cross sections for BF and BF_2 such as elastic, excitation, differential (DCS) and momentum transfer cross sections (MTCS) along with the total ionization cross sections which is compared with the BEB data [10]. Calculations are performed with the complete active space -configuration (CAS–CI) and static exchange (SE) models using the R–matrix and spherical complex optical potential (SCOP) methods. The CAS–CI calculations are performed with increasing number of target states until converged results are obtained. We have used two theoretical methods to carry out calculations in different energy regimes. In the low energy region (<10eV), the *ab-initio* R-matrix method gives a good representation of the electron-molecule

scattering. However, at high energies, a complete theoretical *ab-initio* treatment is not possible since all discrete and continuum channels are open. Consequently, different approximations have to be implemented to make computations manageable. The SCOP method is a simple and powerful tool at intermediate and high energies ($\sim$ 10–2000eV) giving reliable results from diatomic molecules to complex biomolecules. The next section describes these theoretical methods which are used to calculate various cross sections reported in the present work.

2. THE R–MATRIX METHOD

In this work, we have used the R–matrix method [21] to perform low energy electron-molecule scattering calculations. We have used the Quantemol–N [22] to run the UK molecular R–matrix codes [21]. Through the years, R–matrix calculations have been shown to successfully predict accurate cross section data for a number of molecular targets using the Quantemol–N [22–27]. Within the fixed nuclei approximation, the R–matrix theory is primarily constructed on the division of coordinate space into an inner and outer region to treat electron molecule scattering. The inner region contains the target molecule with $N+1$ indistinguishable electrons, where $+1$ indicates the scattering electron. This $N+1$ collision system is treated as a bound state in the inner region, where short-range forces such as electron correlation and exchange are important. The results obtained in the inner region are fed to the outer region which only explicitly considers the scattering electron. In the outer region, the scattering electron is far away from the target electron cloud and exchange and correlation effects are negligible, so only the long–range multipolar interaction between the scattering electron and the target are considered. Here, the inner region is taken to be a sphere of radius 10 a_0 centered on the molecular center–of–mass, while the outer region is extended up to 100 a_0. The radius of the inner region is chosen to contain the wave function of the target within the R–matrix sphere.

The inner region wave functions are constructed using the close–coupling (CC) [28] expansion for the $N+1$ target plus electron system in a fixed-nuclei approximation and is expressed as,

$$\psi_k^{N+1} = A\sum_{ij} a_{ijk}\Phi_i^N(x_1,...,x_N)u_{ij}(x_{N+1}) + \sum_i b_{ik}\chi_i^{N+1}(x_1,...,x_{N+1}). \quad (1)$$

In the above equation, the first summation runs over the target states times continuum orbitals used in the close-coupled expansion. A is the anti–symmetrization operator which ensures that the Pauli principle is obeyed by the electrons. Φ_i^N is the wavefunction of the i^{th} target state, x_N is the spatial and spin coordinate of the N^{th} target electron and u_{ij} are the continuum orbitals which represent the scattering electron. The continuum orbitals are positioned at the center–of–mass of the molecule. Moreover, they are long-ranged compared to the orbitals centered at the nuclei and thus have amplitude on the R–matrix boundary. In the second term, the $\chi_i^{(N+1)}$ are called L^2 configurations, which accounts for the short-range correlations and polarization effects.

These χ_i are multi–center quadratically integrable functions constructed by placing all the $N+1$ electrons in the target molecular orbitals (MOs). a_{ijk} and b_{ik} are the variational coefficients which are determined by the diagonalization of the Hamiltonian matrix.

In the present calculations, the target molecular orbitals (both occupied and virtual orbitals) were constructed employing the Hartree-Fock Self–Consistent Field method with Gaussian type orbitals (GTOs); the continuum orbitals used were the GTOs of Faure et al. [29]. The R–matrix links the inner region to the outer region. It is constructed at the boundary of these two regions using the inner region solution. This R–matrix was then propagated outwards and matched with known asymptotic scattering functions obtained from a Gailitis expansion [30]. Matching to the asymptotic boundary conditions gives the K–matrix which is a symmetric matrix that contains all the information about the scattering process. In particular, the eigenvalues of the K–matrices gives the eigenphase sum (δ) whose expression is given as follows,

$$\delta = \sum_i \arctan(K_{ij}). \tag{2}$$

The summation in the above equation runs over all the open channels. These K-matrices are then employed to obtain the T-matrices. The T-matrices are used to obtain various scattering observables and cross sections. T-matrix can be evaluated from the K-matrices using the definition,

$$T = \frac{2iK}{1 - iK}. \tag{3}$$

The POLYDCS program of Sanna and Gianturco [31] was used to calculate the DCS and MTCS. Resonances were detected using the RESON [32] program (available within the R–matrix suite) by automated fitting to a Briet–Wigner profile [33] to obtain their energies and widths. The detailed discussion of the R-matrix method is available elsewhere [21, 34] and here we have chosen only the basic equations for brevity.

Here, we have used two scattering models (SE and CAS-CI) in the R-matrix method to describe the scattering processes and to determine the electronic wavefunction of the target. The type of scattering model depends on the choice of target electronic states and L^2 functions included in equation 1. In the SE model, the target electrons are kept in the ground state configuration (also known as frozen electrons). SE configurations use Hartree-Fock Self-Consistent Field (HFSCF) target wavefunctions and are not allowed to be polarized by the incident electron. However, this method is well suited to detecting shape resonances where the scattering electron is temporarily trapped behind a potential barrier created by the molecule. The SE approximation cannot detect Feshbach/core-excited or mixed resonances which involve excitation of bound electrons. The CAS-CI model is a more sophisticated approximation than SE, where many electronically excited states of the target (active electrons) are included in the expansion of equation 1. The inclusion of more excited states increases the polarization effects which make these calculations accurate. These calculations identify both the shape and Feshbach/core-excited resonances fairly well along with the calculation of excitation cross sections.

This calculation is performed with the CC approximations. The products of this model are called Configuration State Functions (CSFs). A full analysis of the behaviour of CAS-CI method is given elsewhere [35].

2.1. Target models for BF and BF_2 used in the present calculations

BF has a linear structure with a bond distance of 1.267 Å [36] between the boron and fluorine atoms belonging to the $C_{\infty v}$ point group symmetry. The structure of BF_2 was optimized using the Gaussian 09 [37] suite, as its geometry was not available in the CCCBDB website. BF_2 has a bent structure with two fluorine atoms attached to boron atom with a bond length of 1.30 Å belonging to the C_{2v} natural point group symmetry. The calculation for both the targets was carried out in the C_{2v} point group symmetry as Quantemol-N, in common with nearly all other electronic structure codes, cannot handle non-Abelian point groups such as $C_{\infty v}$. The CAS–CI and SE calculation are performed with a cc–pVTZ basis set for both the systems. The ground state electronic configuration of the BF is given as, $1a_1^2$, $2a_1^2$, $3a_1^2$, $4a_1^2$, $1b_2^2$, $1b_1^2$, $5a_1^2$ ($1\sigma^2$, $2\sigma^2$, $3\sigma^2$, $4\sigma^2$, $1\pi^4$, $5\sigma^2$ in $C_{\infty v}$ symmetry), while the electronic ground state configuration of BF_2 in its equilibrium geometry is given as $1b_2^2$, $1a_1^2$, $2a_1^2$, $3a_1^2$, $2b_2^2$, $4a_1^2$, $3b_2^2$, $5a_1^2$, $1b_1^2$, $1a_2^2$, $4b_2^2$, $6a_1^1$. For each molecule, the CSFs are generated by keeping some electrons 'frozen' in the core and considering all configurations arising by distributing the remaining electrons in the CAS. In the CAS–CI calculation for BF out of 14 electrons, 6 electrons are frozen in $1a_1$, $2a_1$, $3a_1$ (1σ, 2σ, 3σ) molecular orbitals and 8 electrons are in the active space of $4a_1$, $5a_1$, $6a_1$, $7a_1$, $1b_1$, $2b_1$, $1b_2$, $2b_2$ (4σ, 5σ, 6σ, 7σ, 1π, 2π) molecular orbitals. For BF_2, out of 23 electrons, 16 electrons are frozen in the molecular orbitals $1a_1$, $2a_1$, $3a_1$, $4a_1$, $5a_1$, $1b_2$, $2b_2$, $3b_2$ and 7 electrons are active in the 7 molecular orbitals $6a_1$, $7a_1$, $1b_1$, $2b_1$, $4b_2$, $5b_2$, $1a_2$. In our CAS–CI model, 49 and 20 target states have been included for the best target model of BF and BF_2 for which the results are converged. For these target models of BF and BF_2, the number of CSF's generated for the ground state are 492 and 196, and the number of scattering channels included in the calculation are 286 and 128 respectively. However, in the SE calculation, all the electrons are frozen in the lowest configuration for both the targets.

The dipole moment of 0.34 au is obtained in the present CAS–CI model for BF which is higher than the experimental data of Lovas and Johnson [38] at 0.19 au. However, our dipole moment is in good agreement with the recent theoretical values of Kobus et al. [39], Magoulas et al. [40] and Fantuzzi et al. [41] who obtained 0.34, 0.33 and 0.36 au respectively. The first vertical excitation energy of BF obtained in the present calculation is 4.47 eV, which is slightly higher than the adiabatic experimental values of 3.61 eV [42], and the R–matrix and MRD–CI calculation at 3.83 eV [43], and 3.57 eV [44] respectively. The vertical excitation energy of the first 10 excited state of BF included in the calculation are given in Table 1. The present results are compared with the previous experimental and the theoretical results and are found to be slightly higher than the previous results in general for all the states. The absolute ground state

energy obtained is -124.1754 Hartree, which is in good agreement with the theoretical value of Kobus et al. [39] at -124.1687 Hartree.

Table 1. Vertical excitation energy of BF in comparison with available data in eV; the experimental values are adiabatic.

States	**Present**	**Experiment** [42]	**Theory**	
$X^1\Sigma^+$	0	0	R–matrix [43]	MRD–CI [44]
$^3B_1$, $^3B_2$ (a $^3\Pi$)	4.47	3.61	3.83	3.57
$^1B_1$, $^1B_2$ (A $^1\Pi$)	7.15	6.34	6.93	6.56
$^3A_1$ (b $^3\Sigma^+$)	9.34	7.56	7.63	7.52
$^1A_1$ (B $^1\Sigma^+$)	9.92	8.10	8.14	7.98
$^3A_1$ (c $^3\Sigma^+$)	10.96	8.31	8.34	8.20
$^3A_2$ ($^3\Sigma^-$)	13.08	–	–	–
$^1A_1$ ($^1\Sigma^+$)	13.50	–	–	–

Table 2. Vertical excitation energies for BF_2 in comparison with available data in eV.

States	**Energy (eV)**	**Others**
$^2A_1$	0	–
$^2B_1$	6.44	3.24 [45]; 4.66 [46]
$^2B_2$	10.55	–
$^2A_1$	10.93	–
$^2A_2$	12.26	–
$^2B_2$	12.44	–
$^4B_2$	13.03	–
$^4A_2$	13.08	–
$^2B_1$	13.4	–
$^2A_2$	13.43	–
$^2B_2$	13.79	–
$^4A_1$	14.23	–
$^2A_1$	15.19	–
$^2A_2$	15.52	–
$^2B_2$	15.58	–

In the case of BF_2, the dipole moment obtained in the present CAS–CI calculation is 0.23 au, which is in good agreement with the experimental data of Rothenberg at 0.27 au [47]. The absolute ground state energy obtained with this model is -223.7094 Hartree, which is in reasonable agreement with the ground state energy of Cai [45] at -224.0715 Hartree. The first excitation energy of BF_2 is reported at 6.44 eV with the present target

model and is quite high with respect to the data of Cai [45] and Atkinson et al. [46] at 3.24 and 4.66 eV respectively. For both BF and BF_2 the vertical excitation energies are in general higher than other values. The reason for such behavior may be attributed to the use of HFSCF molecular orbital (MOs). The use of HFSCF MOs for multistate calculations tends to over-emphasize the ground state at the expense of excited states, leading to excitation energies which are too high [21]. However, we also note that experimental values are usually for adiabatic excitation which allows for relaxation of the geometry of the excited state compared to vertical excitation considered here which does not allow for this effect. The vertical excitation energy of the first 15 excited states of BF_2 included in the calculation is given in Table 2.

3. SPHERICAL COMPLEX OPTICAL POTENTIAL (SCOP) METHOD

In the present work, we have used the spherical complex optical potential (SCOP) method to predict the elastic and MTCS at intermediate energies (up to 2000 eV). A detailed description of this method can be obtained from our previous articles [27, 48–51]. Here, we present an overview of the calculation.

The interaction between the incoming electron and the target molecule is represented by a complex optical potential ($V_{opt}(r, E_i)$), given as

$$V_{opt}(r, E_i) = V_R(r, E_i) + i\, V_I(r, E_i). \tag{4}$$

E_i is the energy of the incident electron. This potential is used to solve the Schrödinger equation to obtain phase shifts (δ_l) which contains the entire information about the scattering event. In the present work, we have used the Hartree–Fock wavefunction of Cox and Bonham [52] to calculate the charge density and static potential. To include the exchange effect, the parameter–free Hara's free–electron gas exchange model [53] is used whereas the correlation–polarization potential is obtained using the model potential of Zhang et al. [54]. These three interaction potentials constitute the real part of the complex potential ($V_R(r, E_i)$) and thus provide for all the elastic phenomena occurring during the scattering event. The imaginary part of the potential ($V_I(r, E_i)$) (also known as the absorption potential) accounts for the inelastic events and in this work it is represented by the quasi–free model of Staszewska et al. [55]. The working formulae related to the calculation of elastic and MTCS are given as,

$$Q_{el}(E_i) = \frac{\pi}{k^2} \sum_{l=0}^{\infty} (2l+1) \left| \eta_l \exp(2iRe\, \delta_l) - 1 \right|^2 \tag{5}$$

and

$$Q_{mtcs}(k) = \frac{4\pi}{k^2} \sum_{l=0}^{\infty} (l+1) \sin^2[\delta_{l+1}(k) - \delta_l(k)]. \tag{6}$$

Where, η_l is the inelasticity factor given as $\eta_l = \exp(-2Im\, \delta_l)$, k is the wave vector associated with the scattered wave and l is the number of partial waves. Other details of the method can be obtained from our previous article [51].

The total ionization cross section (Q_{ion}) is also calculated using the complex scattering potential-ionization contribution (CSP-ic) method [56]. In this, the Q_{ion} is derived from the inelastic cross section (Q_{inel}) which is the sum of all the allowed electronic excitation cross section (Q_{exc}) and Q_{ion}. However, to calculate Q_{ion} from Q_{inel} an energy-dependent ratio of cross section is taken which obeys certain boundary conditions [56]. It has been found that the relative contribution of ionization at peak for stable target molecules is around 70-80% of the inelastic cross section [56]. Therefore, an empirical value for the relative contribution of Q_{ion} is selected at the peak of Q_{inel}. We have chosen the value of $R_p = 0.75$ for all the targets in the present case. The deviation in the cross section by choosing the ratio 0.7 and 0.8 with respect to 0.75 is about 7% at the peak.

The bond lengths of the present targets are comparable to the added radii of B and F atoms. Hence, the molecular charge density of these targets is obtained as the sum of the charge densities of the constituent atoms. With the help of this method, we have computed the above–mentioned potentials and charge density of the entire molecule and hence the required cross section. The ionization potential of BF and BF_2 used in the present calculations are 11.12 eV [36] and 8 eV [57] respectively. The polarizability of the targets has been calculated in the present study by fully optimizing the geometry of the molecule using the Gaussian package [37]. The target properties used for the intermediate to high energy calculations are given in Table 3.

Table 3. Target properties

Target	**Polarizability($Å^3$)**	**Ionization potential (eV)**	**Bond length ($Å$)**
BF	3.034 (Present)	11.12 [36]	1.2699 [36]
BF_2	2.732 (Present)	8.00 [57]	1.3006 [36]

Table 4. Resonance position and width for BF and BF_2 detected in the present calculations for 49 and 20 state calculations respectively.

	States	**Resonances**	
		Position (eV)	**Width (eV)**
BF	$^2A_1$ ($^2\Sigma^+$)	4.84	0.51
	$^2A_2$ ($^2\Sigma^-$)	4.71	0.59
	$^2B_1$, $^2B_2$ ($^2\Pi$)	0.52	0.62
BF_2	$^3B_1$	1.73	2.42
	$^3B_1$	6.45	0.00008

4. RESULTS AND DISCUSSIONS

In this section, we present and discuss the results obtained in the present calculation. Table 4 provides the resonance states along with their respective position and widths for each target.

4.1. Results for BF

The elastic cross section and MTCS for BF is shown in Figure 1 for 49, 40, 20, 10, and 5 states along with SE R–matrix calculation at low energies till 10 eV using the cc–pVTZ basis set. Above 10 eV, intermediate to higher energy calculations are performed with the SCOP method. The cross section calculated using the two methods join smoothly around 10 eV, which allows us to provide cross section over a wide energy range from 0.1 to 2000 eV. This also justifies the use of the two theories at two energy regimes. Below 10 eV, the resonances are detected at 0.52, 4.71, 4.84 eV due to the $^2\Pi$, $^2\Sigma^-$, and $^2\Sigma^+$ scattering states in 49 target state calculations. At energies below 1 eV, an enhancement is seen in both elastic and MTCS due to the resonance present at 0.52 eV energy for the 49 state calculation. The resonances detected at 4.71 and 4.84 eV due to $^2\Sigma^-$ and $^2\Sigma^+$ states are quite clearly seen in the MTCS but are not visible in the elastic cross section. The low-lying $^2\Pi$ state resonance is of shape character, similar to the well-known $^2\Pi$ resonance found in electron collisions with the isoelectronic CO molecule. The other two resonances, of $^2\Sigma^-$ and $^2\Sigma^+$ symmetry, are of Feshbach character. A Feshbach resonance is formed when the incoming electron is temporarily trapped by an excited state forming a temporary, excited negative ion state. Feshbach resonances are generally longer-lived (narrower) than shape resonances. The shape and nature of the cross sections for SE, 5, 10, 20, 40 and 49 target states give quite a similar cross section except that the resonance peak due to $^2\Pi$ resonance state which shifts to lower energies as the number of target states is increased. The calculated cross sections for the 40 and 49 states show similar results and hence the calculation can be said to have obtained convergence. The magnitude of the peak also increases as the number of states is increased from 5 to 49 states. The SE calculation, which does not incorporate polarization effects, shows a resonance at around 2 eV compared to 0.52 eV in the 49 state calculation. The variation of cross section in the energy range of $0.1 \sim 1$ eV for different target states along with the SE calculation can be attributed to the electron correlation and polarization effects which becomes important at these energies. The results for 49-state calculations are mostly converged and this was the maximum number of target states that could be included for the choice of our complete active space (CAS). For all the calculations below 0.5 eV, the cross section shows a sharp rise which can be attributed to the long–range potential associated with the permanent dipole moment of the BF which results in strong forward scattering at low energies. The dipole potential is long-range and its dependence is $\sim \frac{1}{r^2}$. Because of this, the elastic cross section behaves as $\sim \frac{1}{E^2}$, where E is the incident energy. Clearly, when E is close to zero, the cross section should be large. Similarly, the DCS is also inversely proportional to the square of an angle-dependent

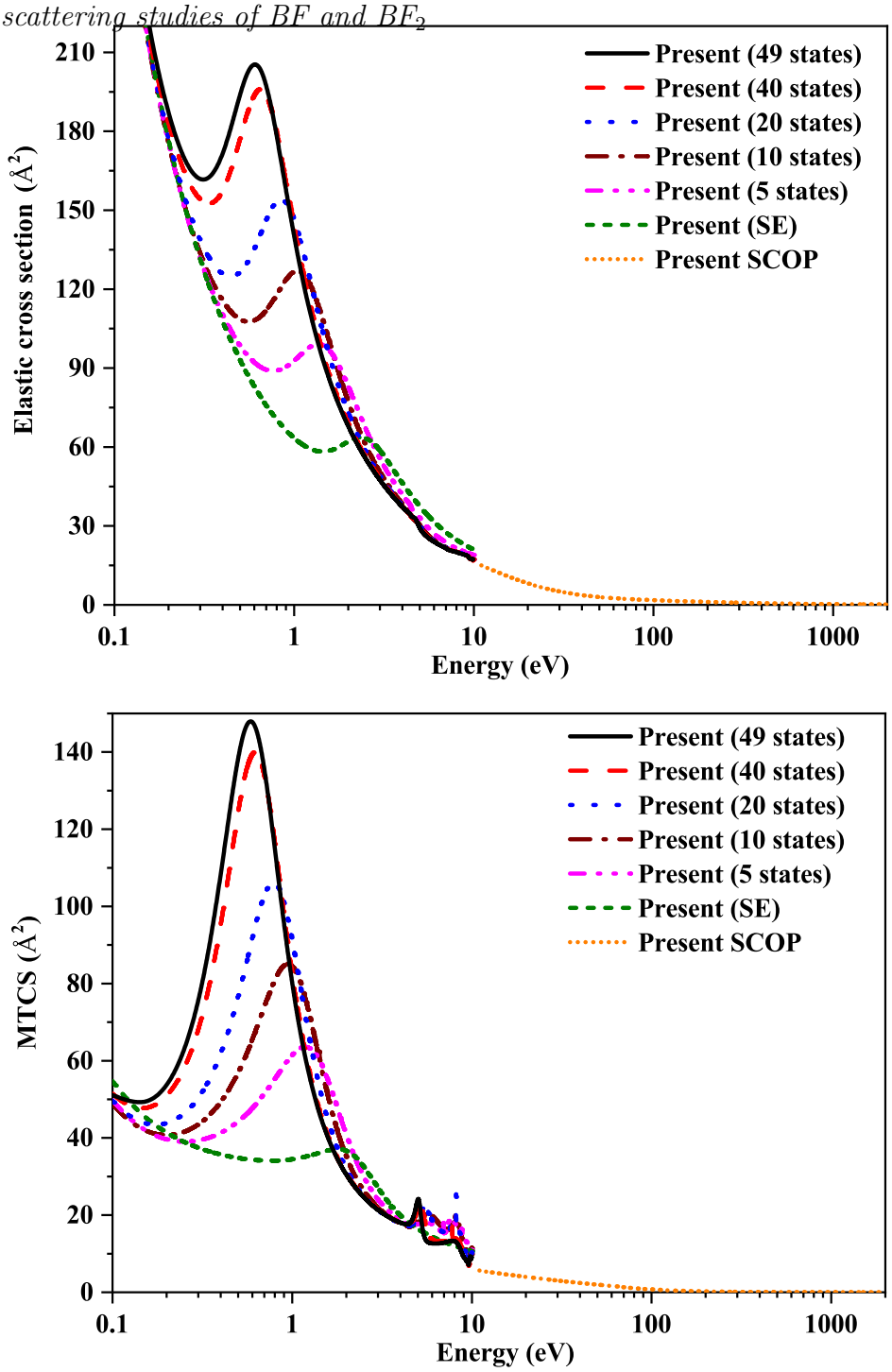

Figure 1. Elastic cross section and MTCS for 49, 40, 20, 10, and 5 states and static exchange R–matrix calculation at low energies; SCOP calculation at intermediate and higher energies of BF.

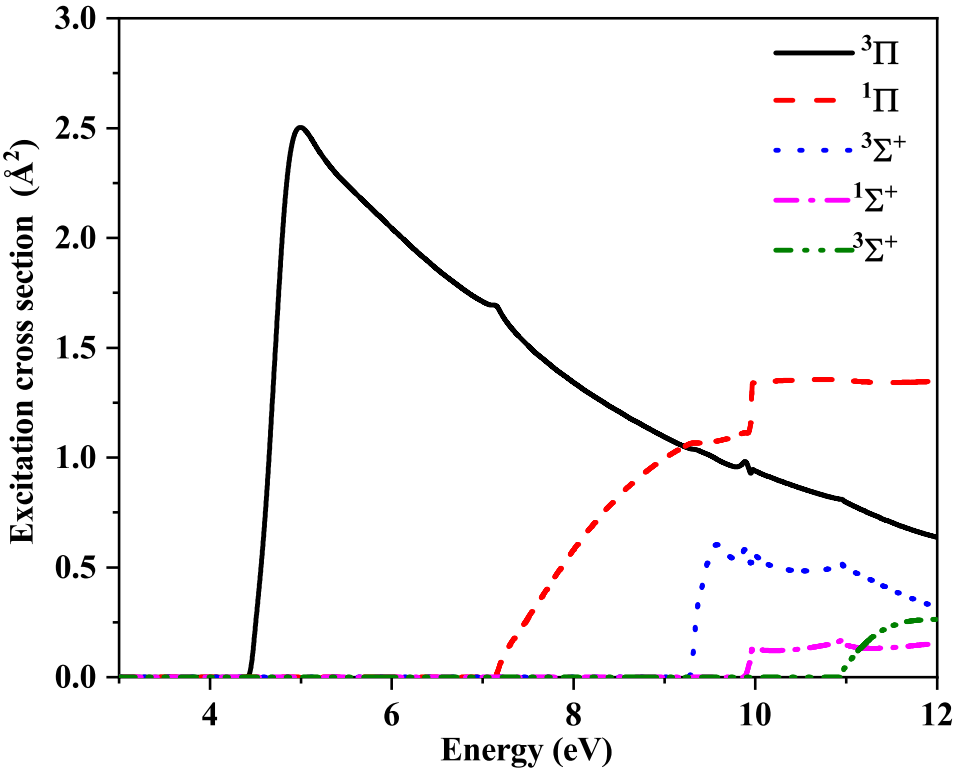

Figure 2. Excitation cross section from the ground state for 5 low lying excited states of BF for the 49 states calculation.

quantity which vanishes for the forward direction $\theta = 0$ and hence the differential cross section should be large for forward scattering; see the discussion of the DCSs below. A full discussion of this issue is given by Zhang et al. [58]. Since the target is polar, a Born correction is used to correct the effects of the dipole in the scattering. The MTCS also follows a similar trend to that of the elastic cross section in terms of the shape and nature of the cross sections for different target state calculations. It is also seen that for MTCS, the SCOP data shows significant value only up to 200 eV, beyond which the MTCS seems to die out with increasing incident energy.

Figure 2 shows the excitation cross section from the ground state for the five low-lying excited states of BF. The excitation threshold for each of the states can be obtained from Table 1. As evident from the figure, excitation to the $^3\Pi$ state has the largest cross section followed by excitation to the $^1\Pi$ state. The triplet states have the maximum cross sections due to their lower threshold. The sharp rise in the excitation cross section of $^3\Pi$ at around $4 \sim 6$ eV may be due to the presence of Feshbach/core-excited resonances at these energies. No previous study is available in the literature to compare with the present data.

The elastic DCS for BF at energies of 0.1, 1, 3, 5, 7, 10, and 15 eV are plotted together in Figure 3. The DCS represents the angular change of the electron trajectory when scattered from an isotropic distribution of the target molecule; such cross sections

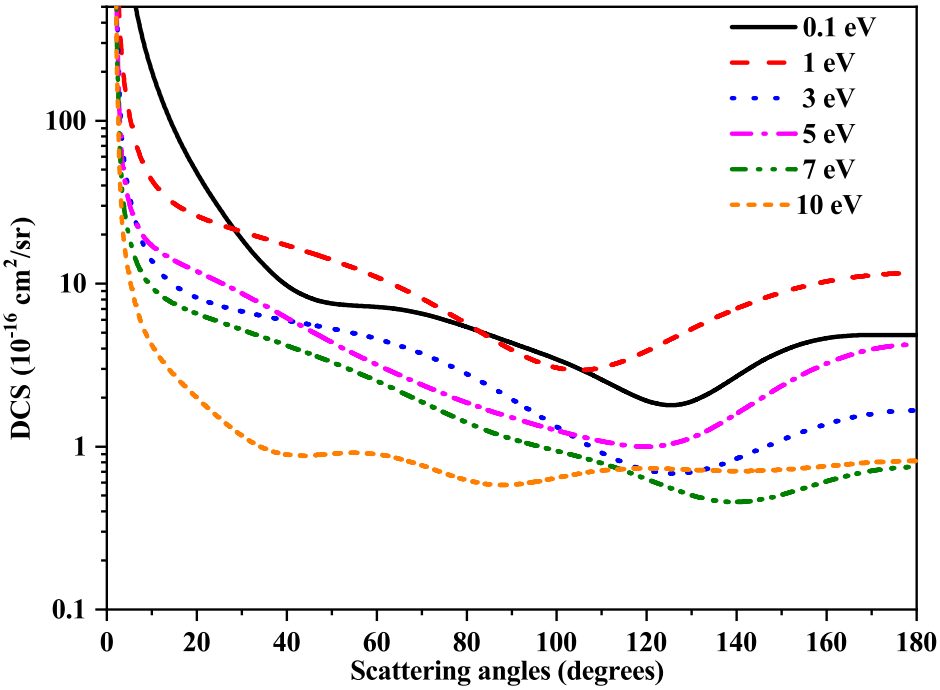

Figure 3. Elastic DCS for BF at energies, 0.1, 1, 3, 5, 7, and 10 eV for 49 states calculations.

are thus useful in plasmas where the electrons are initially in a collimated beam. For forward scattering at very low angles below 5 degrees, the DCS rises sharply due to the large dipole moment of BF. The magnitude of the DCS decreases with increase in the energy. Since there is no previous available data for comparison, there is an urgent need for more investigation into this system by other groups to validate the present results and update the study of this important plasma gas with a recommended datasets. The present results could be a useful input data for plasma simulation and for comparing with other results.

4.2. Results for BF_2

The elastic cross section and MTCS is plotted in Figure 4 for the 20, 15, and 5 states CAS–CI model calculations along with the SE model R–matrix calculation of BF_2 at low energies until 7 eV. Below 7 eV, resonances are detected at 1.73 and 6.45 eV with a width of 2.41 eV and 0.8 x10^{-4}, respectively, both due to the $^3B_1$ scattering state. These resonances can also be seen in the elastic and MTCS at the same energy as a broad peak. The 1.73 eV resonance is of shape character with a broad width and the resonance at 6.45 eV detected just above the first excitation energy is of Feshbach character with a very narrow width. The results are quite similar for all the different target state calculations except that the low energy resonance shifts to higher energies for SE and 5 states calculation compared to 15 or 20 states calculations in the elastic

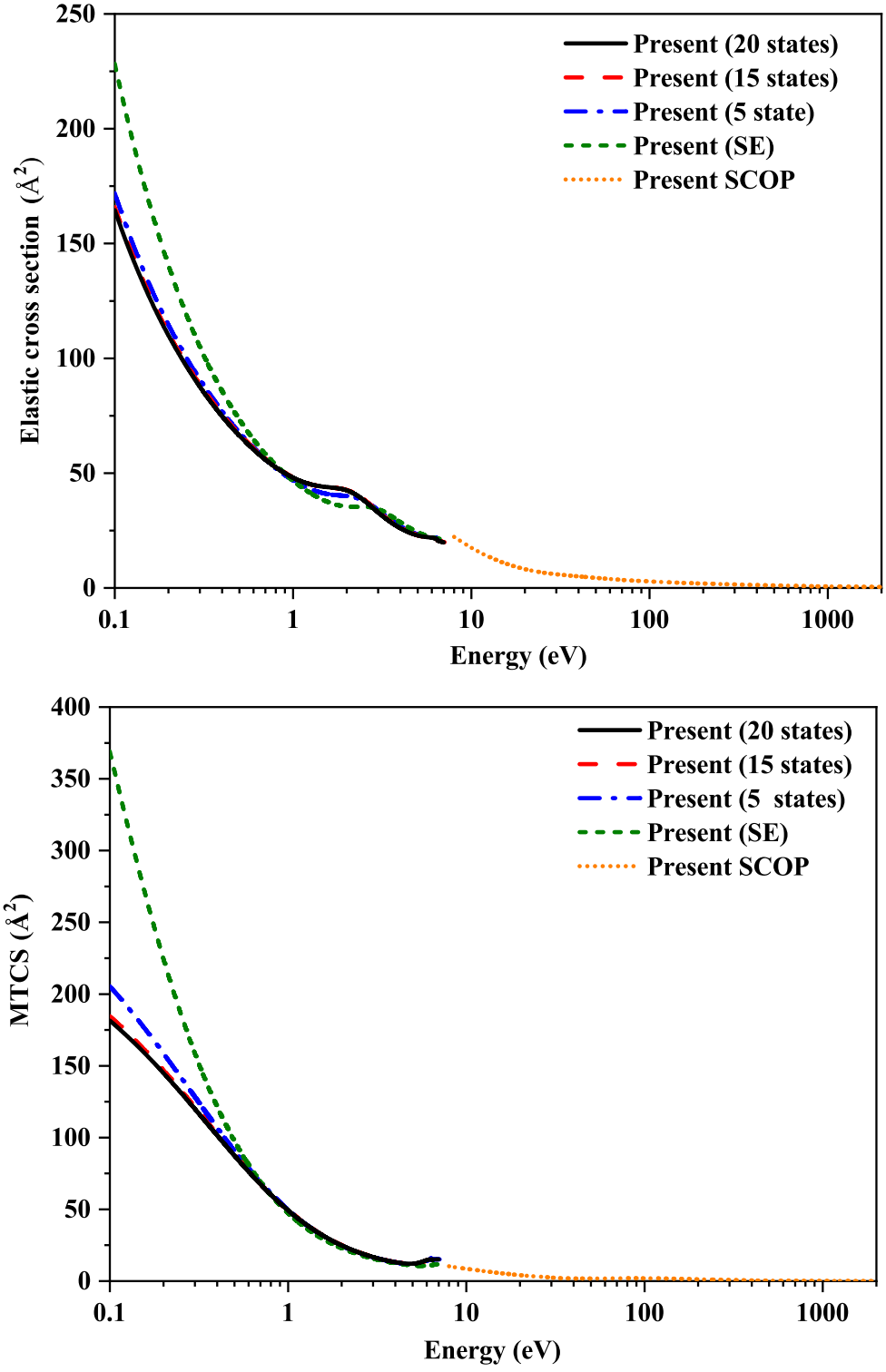

Figure 4. Elastic cross section and MTCS for 20, 15, 5 states and SE R–matrix calculation at low energies; SCOP calculation at intermediate and higher energies of BF_2

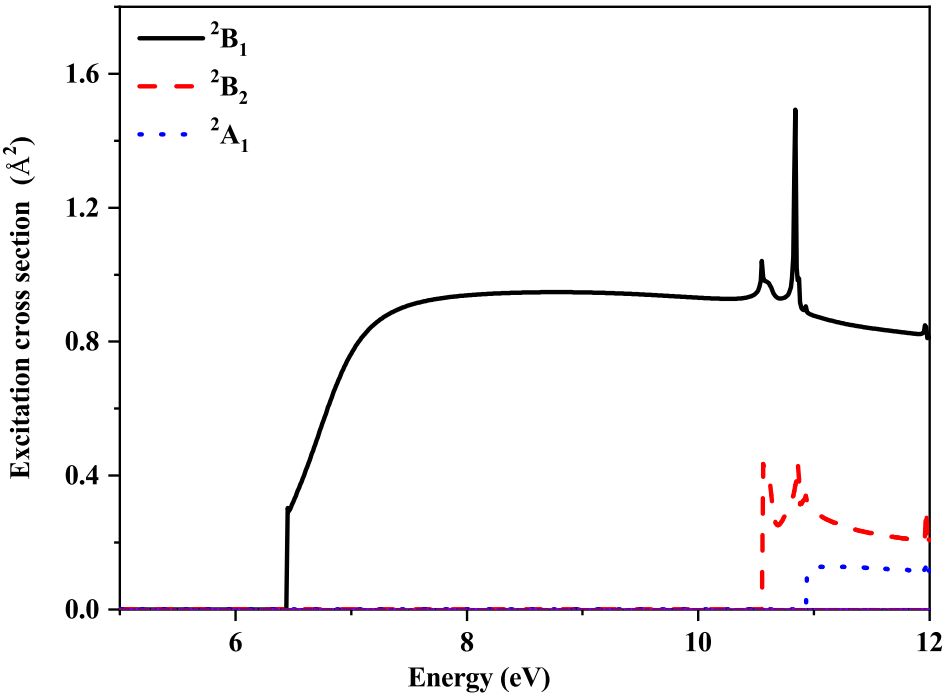

Figure 5. Excitation cross section of BF_2 from its ground state for 3 low lying excited states for a 20 state R–matrix calculation.

cross section. The results have converged for 15 and 20 state calculations. The MTCS is also quite similar for 15 and 20 target states calculations, whereas the SE and 5 state results show some variation for energies below 0.5 eV. The resonance feature is also seen in the MTCS at 6.45 eV. However, the resonance feature at 1.73 eV as detected in the present study by the RESON program is not seen in the MTCS but can be seen in the elastic cross section. As before, we also plot the SCOP data. For both the elastic and momentum transfer cross section curve, we see a reasonable overlap between the data obtained from both the theories (R–matrix and SCOP) at around 7 to 8 eV.

The excitation cross section for the three low-lying excited states, $^2B_1$, $^2B_2$ and $^2A_1$ are plotted in Figure 5. The threshold for the first excitation energy is at 6.44 eV and the maximum contribution to the total cross section is given by the first ($^2B_1$) excited state cross section with a maximum of 1.4 $\mathring{A}^2$ at around 11 eV, which may be due to its lower threshold. The thresholds for the second and third excited states are at 10.55 and 10.93 eV respectively and the contributions from these states are significantly lower than the first state. The structures at around 11 eV are possibly some kind of pseudo resonance.

The elastic DCS for BF_2 at energies 1, 3, 5, 7, and 10 eV are plotted together in Figure 6. Besides 1 eV, all the results are quite similar among each other with a minimum of the DCS seen for 7 eV at an angle of 100 degrees approximately. At a very low angle, the DCS shows a sharp rise in the cross section due to the dipole moment of the BF_2. There is a need for more investigation into this system theoretically and

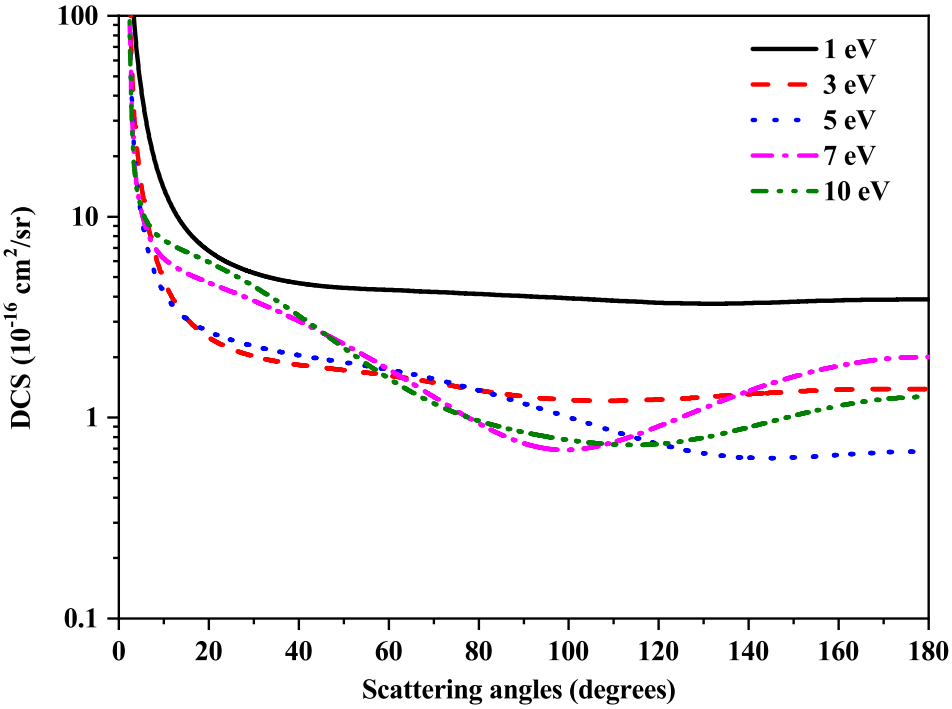

Figure 6. Elastic DCS of BF_2 for 1, 3, 5, 7 and 10 eV for a 20 state R–matrix calculation.

experimentally due to the lack of available data in the literature.

The total ionization cross section for BF and BF_2 are calculated using the SCOP and CSP-ic method in the energy range from the ionization threshold to 5 keV. The results are compared with the BEB data [10] and are plotted together in Figure 7. For BF, the present results show good agreement with the BEB data throughout the energy range. However, for BF_2, the agreement with the BEB data is good only from threshold till 40 eV after which the present cross section is lower than the BEB estimate. We do not know the precise reason for this discrepancy for BF_2 at intermediate and higher energies.

The elastic cross section of BF, BF_2, and BF_3 at low energies below 10 eV are plotted together in Figure 8 to get an overall idea about the shape and nature of the cross section along with the resonances detected at these energies. Due to the large dipole moments of BF and BF_2, the corresponding cross section show a sharp rise at energies below 0.5 eV. Since BF_3 is a symmetric molecule with D_{3h} symmetry with no dipole moment, its cross section does not show a sharp rise at low energies as seen for BF and BF_2. Shape resonances are detected for BF, BF_2, and BF_3 at low energies below 10 eV are at 0.52, 1.73, and 3.79 eV respectively. The magnitude of the elastic cross section also decreases as one goes from BF to BF_2 and to BF_3, which can be attributed to the addition of fluorine atoms to the molecule as we go from BF to BF_3. Such fluorination effect has already been seen in the elastic cross section where the magnitude of the cross section goes down with the addition of fluorine atom and it also shifts the resonance

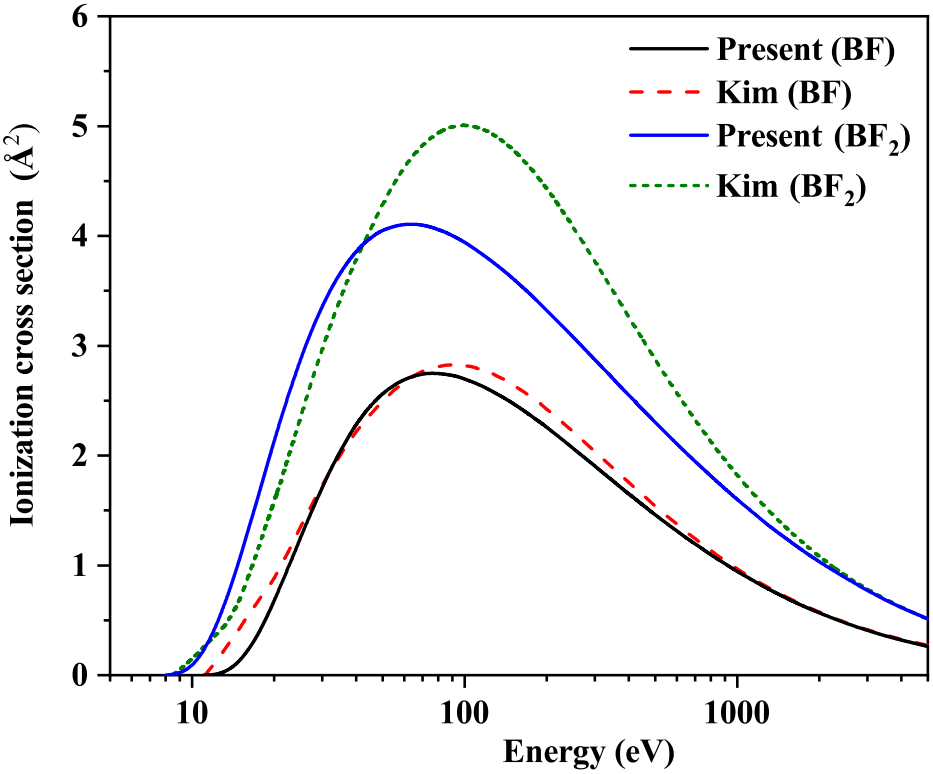

Figure 7. Total ionization cross section of BF and BF_2 calculated using the SCOP and CSP-ic and compared with the BEB data of reference [10]

position to higher energies [59]. All the results seem to converge beyond 8 eV for BF, BF_2, and BF_3.

5. CONCLUSIONS

In this work, we have investigated in detail a set of scattering cross sections for electron collision with BF and BF_2 radicals. Most of the cross sections for these target systems are investigated for the first time, which are essential data for modeling the BF_3 plasma as mentioned in the introduction. The low energy cross sections are investigated using the *ab-initio* R–matrix method whereas the elastic and MTCS are extended to higher energies with the help of SCOP calculations. Various target and scattering models are considered for BF and BF_2 to get the best values of cross sections as there are no results available in the literature. The resonances are identified along with their widths at low energies for both the systems.

Our previous study [17] of the BF_3 molecules using a similar approach have shown good agreement of the elastic cross section with the experimental [4] as well as the theoretical data [15]. This gives us the confidence that the elastic cross sections calculated for BF and BF_2 using a similar methodology are reliable. The inelastic excitation cross section may not be very accurate since the calculated threshold for the

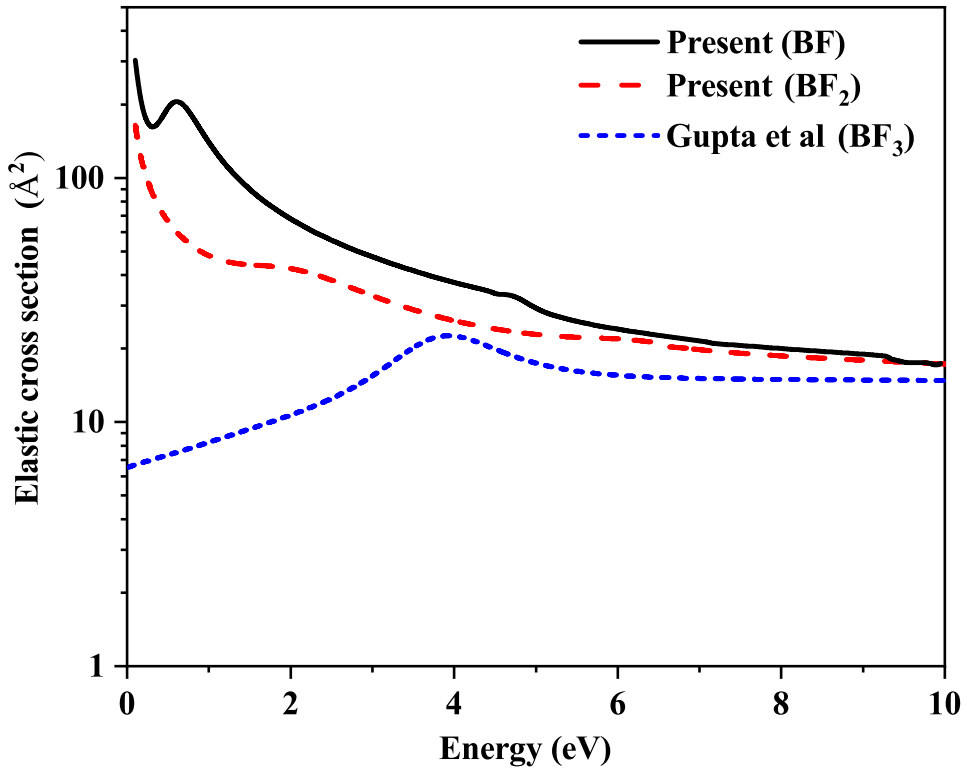

Figure 8. Elastic cross section of BF, BF_2 and BF_3 for a 49 state, 20 state and 15 state R–matrix calculation at low energies till 10 eV. BF and BF_2 are the present calculations and BF_3 data are taken from our previous R–matrix calculations by Gupta et al. [17]

various excited states differs quite a lot from previous studies. This may be due to the use of HFSCF MOs used in the present study which does not model the excited states accurately. However, this may be a good starting point for other theoretical groups to study these radicals for elastic and inelastic processes. Further experimental and theoretical studies are encouraged with this work, which in turn could help in the validation of the present data.

Data Availability

The data that supports the findings of this study are available within the article [and its supplementary material].

Acknowledgements

D.G. is pleased to acknowledge the support of this research to the National Fusion Research Institute (NFRI), Korea for the research grant and scholarship.

References

[1] Stojanović V, Raspopović Z, Jovanović J, Radovanov S, Nikitović Ž and Petrović Z L 2012 *Nuclear Instruments and Methods in Physics Research Section B: Beam Interactions with Materials and Atoms* **279** 151–154

[2] Oh S H, Ma J W, Bae J M, Kang Y s, Ahn J P, Kang H K, Chae J, Suh D, Song W, Kim S *et al.* 2017 *Applied Surface Science* **419** 1–8

[3] Kwok D T, Chu P K, Takase M and Mizuno B 2001 *Surface and Coatings Technology* **136** 146–150

[4] Hoshino M, Limão-Vieira P, Suga A, Kato H, Ferreira da Silva F, Blanco F, García G and Tanaka H 2015 *The Journal of chemical physics* **143** 024313

[5] Gu S, Kang H J, Kwon D C, Kim Y S, Chang Y M and Chung C W 2016 *Physics of Plasmas* **23** 063506

[6] Kim J H, Kwon D C and Chung C W 2020 *Journal of Vacuum Science & Technology B, Nanotechnology and Microelectronics: Materials, Processing, Measurement, and Phenomena* **38** 022801

[7] Bartschat K and Kushner M J 2016 *Proc. Nat. Acad. Sci.* **113** 7026–7034

[8] Tronc M, Malegat L, Azria R and Le Coat Y 1982 *Journal of Physics B: Atomic and Molecular Physics* **15** L253

[9] Tossell J, Moore J and Olthoff J K 1986 *International Journal of Quantum Chemistry* **29** 1117–1126

[10] Kim Y K and Irikura K K 2000 Electron-impact ionization cross sections for polyatomic molecules, radicals, and ions *AIP Conference Proceedings* vol 543 (American Institute of Physics) pp 220–241

[11] da Costa R F, Ferreira L G, Lima M A and Bettega M H 2003 *The Journal of chemical physics* **118** 75–82

[12] Szmytkowski C, Piotrowicz M, Domaracka A, Kłosowski Ł, Ptasińska-Denga E and Kasperski G 2004 *The Journal of chemical physics* **121** 1790–1795

[13] Radmilovic-Radjenovic M, Varambhia H, Vranic M, Tennyson J and Petrovic Z L 2008 *Publications de l'Observatoire Astronomique de Beograd* **84** 57–60

[14] Vinodkumar M, Korot K, Limbachiya C and Antony B K 2008 *Journal of Physics B: Atomic, Molecular and Optical Physics* **41** 245202

[15] Pastega D F, da Costa R F, Lima M A and Bettega M H 2014 *The European Physical Journal D* **68** 20

[16] Hughes P P, Beasten A, McComb J C, Coplan M A, Al-Sheikhly M, Thompson A K, Vest R E, Sprague M K, Irikura K K and Clark C W 2014 *The Journal of chemical physics* **141** 194301

[17] Gupta D, Chakrabarti K, Yoon J S and Song M Y 2017 *Physics of Plasmas* **24** 123511

[18] Mezei J Z, Colboc F, Pop N, Ilie S, Chakrabarti K, Niyonzima S, Lepers M, Bultel A, Dulieu O, Motapon O *et al.* 2016 *Plasma Sources Science and Technology* **25** 055022

[19] Chakrabarti K and Tennyson J 2009 *Journal of Physics B: Atomic, Molecular and Optical Physics* **42** 105204

[20] Kim Y K and Rudd M E 1994 *Phys. Rev. A* **50**(5) 3954–3967

[21] Tennyson J 2010 *Phys. Rep.* **491** 29 – 76 ISSN 0370-1573

[22] Tennyson J, Brown D B, Munro J J, Rozum I, Varambhia H N and Vinci N 2007 *J. Phys: Conf. Ser.* **86** 012001

[23] Harrison S and Tennyson J 2012 *Journal of Physics B: Atomic, Molecular and Optical Physics* **45** 035204

[24] Barot A, Gupta D, Vinodkumar M and Antony B 2013 *Physical Review A* **87** 062701

[25] Gupta D, Naghma R, Goswami B and Antony B 2014 *RSC Advances* **4** 9197–9204

[26] Kaur J, Mason N and Antony B 2016 *Journal of Physics B: Atomic, Molecular and Optical Physics* **49** 225202

[27] Singh S, Gupta D and Antony B 2018 *Plasma Sources Science and Technology* **27** 105014

[28] Arthurs A and Dalgarno A 1960 *Proceedings of the Royal Society of London. Series A. Mathematical and Physical Sciences* **256** 540–551
[29] Faure A, Gorfinkiel J D, Morgan L A and Tennyson J 2002 *Comput. Phys. Commun.* **144** 224 – 241 ISSN 0010-4655
[30] Gailitis M 1976 *J. Phys. B: At. Mol. Phys.* **9** 843
[31] Sanna N and Gianturco F 1998 *Comput. Phys. Commun.* **114** 142 – 167 ISSN 0010-4655
[32] Tennyson J and Noble C J 1984 *Comput. Phys. Commun.* **33** 421
[33] Breit G and Wigner E 1936 *Physical review* **49** 519
[34] Burke P 2013 *R-Matrix Theory of Atomic Collisions: Application to Atomic, Molecular and Optical Processes* Springer Series on Atomic, Optical, and Plasma Physics (Springer Berlin Heidelberg) ISBN 9783642267581
[35] Tennyson J 1996 *J. Phys. B: At. Mol. Phys.* **29** 6185–6201
[36] CCCBDB **NIST** URL `https://cccbdb.nist.gov/`
[37] Frisch M, Trucks G, Schlegel H, Scuseria G, Robb M, Cheeseman J, Montgomery Jr J, Vreven T, Kudin K, Burant J *et al.* 2013 *There is no corresponding record for this reference.[Google Scholar]*
[38] Lovas F J and Johnson D R 1971 *The Journal of Chemical Physics* **55** 41–44
[39] Kobus J, Moncrieff D and Wilson S 2000 *Physical Review A* **62** 062503
[40] Magoulas I, Kalemos A and Mavridis A 2013 *The Journal of chemical physics* **138** 104312
[41] Fantuzzi F, Cardozo T M and Nascimento M A C 2015 *The Journal of Physical Chemistry A* **119** 5335–5343
[42] Huber K P 2013 *Molecular spectra and molecular structure: IV. Constants of diatomic molecules* (Springer Science & Business Media)
[43] Chakrabarti K, Schneider I and Tennyson J 2011 *Journal of Physics B: Atomic, Molecular and Optical Physics* **44** 055203
[44] Honigmann M, Hirsch G and Buenker R J 1993 *Chemical physics* **172** 59–71
[45] Cai Z L 1993 *International journal of quantum chemistry* **45** 295–301
[46] Atkinson D B, Irikura K K and Hudgens J W 1997 *The Journal of Physical Chemistry A* **101** 2045–2049
[47] Rothenberg S and Schaefer H F 1973 *Journal of the American Chemical Society* **95** 2095–2100
[48] Gupta D and Antony B 2014 *The Journal of Chemical Physics* **141** 054303
[49] Singh S, Naghma R, Kaur J and Antony B 2016 *The Journal of chemical physics* **145** 034309
[50] Gupta D, Choi H, Kwon D C, Yoon J S, Antony B and Song M Y 2017 *Journal of Physics B: Atomic, Molecular and Optical Physics* **50** 085202
[51] Singh S, Sen A and Antony B 2018 *International Journal of Mass Spectrometry* **428** 22–28
[52] Cox H L and Bonham R A 1967 *The Journal of Chemical Physics* **47** 2599–2608
[53] Hara S 1967 *Journal of the Physical Society of Japan* **22** 710–718
[54] Zhang X, Sun J and Liu Y 1992 *Journal of Physics B: Atomic, Molecular and Optical Physics* **25** 1893–1897
[55] Staszewska G, Schwenke D W, Thirumalai D and Truhlar D G 1983 *Phys. Rev. A* **28**(5) 2740–2751
[56] Gupta D, Choi H, Singh S, Modak P, Antony B, Kwon D C, Song M Y and Yoon J S 2019 *The Journal of chemical physics* **150** 064313
[57] Srivastava R and Farber M 1971 *Transactions of the Faraday Society* **67** 2298–2302
[58] Zhang R, Faure A and Tennyson J 2009 *Physica Scripta* **80** 015301
[59] Gupta D, Choi H, Song M Y and Yoon J S 2017 *Chemical Physics Letters* **684** 333 – 338